Operator-splitting errors in coupled reactive transport codes for transient variably saturated flow and contaminant transport in layered soil profiles

D. Jacques [a,*], J. Šimůnek [b], D. Mallants [a], M.Th. van Genuchten [c]

[a] *Waste and Disposal Department, SCK•CEN, Boeretang 200, B-2400 Mol, Belgium*
[b] *Department of Environmental Sciences, A135 Bourns Hall, University of California Riverside,*
900 University Avenue, Riverside, CA 92521, USA
[c] *George E. Brown, Jr. Salinity Laboratory, USDA, ARS, 450 W. Big Spring Rd, Riverside, CA 92507, USA*

Abstract

One possible way of integrating subsurface flow and transport processes with (bio)geochemical reactions is to couple by means of an operator-splitting approach two completely separate codes, one for variably-saturated flow and solute transport and one for equilibrium and kinetic biogeochemical reactions. This paper evaluates the accuracy of the operator-splitting approach for multicomponent systems for typical soil environmental problems involving transient atmospheric boundary conditions (precipitation, evapotranspiration) and layered soil profiles. The recently developed HP1 code was used to solve the coupled transport and chemical equations. For steady-state flow conditions, the accuracy was found to be mainly a function of the adopted spatial discretization and to a lesser extent of the temporal discretization. For transient flow situations, the accuracy depended in a complex manner on grid discretization, time stepping and the main flow conditions (infiltration versus evaporation). Whereas a finer grid size reduced the numerical errors during steady-state flow or the main infiltration periods, the errors sometimes slightly increased (generally less than 50%) when a finer grid size was used during periods with a high evapotranspiration demand (leading to high pressure head gradients near the soil surface). This indicates that operator-splitting errors are most significant during periods with high evaporative boundary conditions. The operator-splitting errors could be decreased by constraining the time step using the performance index (the product of the grid Peclet and Courant numbers) during infiltration, or the maximum time step during evapotranspiration. Several test problems were used to provide guidance for optimal spatial and temporal discretization.
© 2006 Elsevier B.V. All rights reserved.

Keywords: Coupled reactive transport; Unsaturated flow modelling; Geochemical reactions; Operator-splitting errors

---

* Corresponding author.
  E-mail address: djacques@sckcen.be (D. Jacques).

1. Introduction

The migration of many contaminants in the subsurface is affected by a multitude of complex, interactive physical, chemical, mineralogical, geological, and biological processes. Cycles of precipitation and evaporation largely determine if contaminants remain near the soil surface (e.g., Öztürk and Özkan, 2004). Changes in the chemical composition or pH of the soil solution may impact the retention of heavy metals, radionuclides, or other contaminants on organic matter or iron oxides (e.g., Kohler et al., 1996; Meeussen et al., 1998; Kent et al., 2000; Davis et al., 2004). Dissolution and precipitation of minerals generally buffer the transport of a solution with a different pH or chemical composition through the soil profile (e.g., Ayora et al., 1998; Adler, 2001). The mobility of many elements such as arsenic and iron may be further impacted significantly by changes in the redox state resulting from fluctuations in the phreatic surface, or because of temporary saturation of certain soil layers during periods of heavy rainfall. Simulation of these and related processes requires a coupled reactive transport code that integrates the physical processes of water flow and advective–dispersive solute transport with a range of biogeochemical processes.

As discussed by Šimůnek and Valocchi (2002), coupled codes can be developed in several ways such as using specific chemistry or a more general biogeochemistry module. Many existing codes with general geochemistry are limited to solute transport and biogeochemical reactions, while water flow paths have to be calculated outside of the reactive transport code (e.g., CRUNCH, Steefel, 2000; PHREEQC, Parkhurst and Appelo, 1999; PHT3D, Prommer et al., 2003). Other codes, such as HYTEC (van der Lee et al., 2003), allow the velocity field to be calculated internally from the permeability field. Still other models have coupled transport and biochemical reactions with saturated flow (TBC, Schäfer et al., 1998; PHAST, Parkhurst et al., 2004) or variably saturated flow (HYDRUS-2D-CW2D, Langergraber and Šimůnek, 2005). The more advanced codes integrate general (bio)geochemistry models with transient unsaturated flow and transport models. These include the multi-dimensional codes 3DHYDROGEOCHEM (Yeh and Cheng, 1999), CORE[2D] (Samper et al., 2000), MIN3P (Mayer et al., 2002), and RETRASO (Saaltink et al., 2004).

Two approaches exist to solve the coupled equations for transient flow, transport and geochemistry (e.g., see Steefel and MacQuarrie, 1996, for an overview): (1) the operator-splitting approach in which the transport and chemistry equations are solved separately (an overview of operator-splitting schemes is given in Carrayrou et al., 2004), and (2) the one-step global implicit approach in which the transport and chemistry equations are solved simultaneously. The main advantages of the global implicit approach are that (a) all processes are treated simultaneously in the temporal, spatial and chemical domains, (b) the method is mass-conservative, and (c) the approach may lead to better convergence for large time steps, which may be an important consideration for multi-dimensional flow problems (Mayer, 1999; van der Lee and De Windt, 2001). However, the global implicit method is generally quite complex mathematically and its memory requirements can be large.

The main advantages of the operator-splitting approach are that: (a) the method is easy to implement when different codes or modules are coupled (i.e., well-documented and tested codes can be used, while the modules later still be updated), (b) the approach allows one to use different and specific methods for solving the transport and reaction equations (Carrayrou et al., 2004), and (c) the resulting code can be readily modified for parallel computations (Hundsdorfer and Verwer, 1995). A disadvantage is the occurrence of operator-splitting errors resulting from both the operator-splitting approach itself and from the time and spatial discretizations (Carrayrou et al., 2004). Operator-splitting errors have been studied for a range of geochemical problems involving first-order degradation reactions (Kaluarachchi and Morshed, 1995), Monod kinetics (Morshed and Kaluarachchi, 1995; Steefel and MacQuarrie, 1996), non-equilibrium sorption and equilibrium

linear adsorption (Barry et al., 1996), equilibrium nonlinear adsorption (Barry et al., 1997), irreversible and reversible kinetic reactions (Carrayrou et al., 2004) and multicomponent transport with surface complexation (Steefel and MacQuarrie, 1996). All of these studies were carried out for steady-state flow conditions; almost no information about the operator-splitting errors is currently available for transient flow conditions.

The objective of this study was to analyze numerical errors associated with the operator-splitting approach in coupled reactive codes for typical soil-related flow and transport problems, especially for applications involving transient flow and transport in heterogeneous soil profiles. Two benchmark problems were considered for this purpose: (i) a first-order decay chain of linearly or nonlinearly sorbing contaminants during precipitation and evapotranspiration, and (ii) a multicomponent transport problem involving cation exchange reactions in a multi-layered soil profile. Simulations were carried out with the recently developed HP1 code (Jacques and Šimůnek, 2005) for variably-saturated water flow and multicomponent solute transport problems in soils. Results are compared with simulations using HYDRUS-1D (Šimůnek et al., 1998) and CRUNCH (Steefel, 2000, based on the earlier GIMRT/OS3D package of Steefel and Yabusaki, 1996) for the first and second benchmark problem, respectively.

2. Theoretical basis

2.1. Numerical model

The HP1 code (Jacques and Šimůnek, 2005) was used to evaluate the operator-splitting approach for different flow and transport problems. The simulator is the result of coupling the variably-saturated water flow and solute transport model HYDRUS-1D (Version 2.0, Šimůnek et al., 1998) and the geochemical model PHREEQC (Version 2.4, Parkhurst and Appelo, 1999). HP1 combines the unique features of the two original models in one comprehensive tool by containing modules to simulate (1) one-dimensional transient water flow in variably-saturated media, including root water uptake and evaporation, (2) the transport of multiple components with provisions for physical nonequilibrium (dual-porosity type) transport, (3) mixed equilibrium/kinetic geochemical reactions (aqueous speciation, ion exchange, mineral equilibrium), and (4) heat transport. This coupling of HYDRUS-1D and PHREEQC makes HP1 a very flexible tool for addressing a large number of flow and multicomponent transport problems in soils, including problems exhibiting heterogeneity in physical and chemical properties. A full description of the processes, constitutive equations and numerical solution strategies are found in the manuals of HYDRUS-1D (Šimůnek et al., 1998), PHREEQC (Parkhurst and Appelo, 1999) and HP1 (Jacques and Šimůnek, 2005; www.sckcen.be/hp1). The main limitations of the current version 1.0 of HP1 are the absence of diffusion of components in the gas phase, and applicability to only one-dimensional flow and transport problems.

For completeness, the mathematical equations used in the examples discussed in this paper are briefly summarized here. One-dimensional water flow in variably-saturated porous media is described using the Richards equation:

$$\frac{\partial \theta(h)}{\partial t} = \frac{\partial}{\partial x}\left[K(h)\left(\frac{\partial h}{\partial x} + 1\right)\right] - S(h) \tag{1}$$

where h is the water pressure head [L], θ is the volumetric water content [$L^3 L^{-3}$], t is time [T], x is the spatial coordinate [L] (positive upward), S is a sink term [$L^3 L^{-3} T^{-1}$], and K is the unsaturated hydraulic conductivity [LT^{-1}]. The water content and hydraulic conductivity are both nonlinear

functions of the pressure head. One possible way of describing these soil hydraulic properties is with the closed-form expressions of van Genuchten (1980):

$$\theta(h) = \theta_r + \frac{\theta_s - \theta_r}{(1 + |\alpha h|^n)^m} \tag{2}$$

$$K(h) = K_s S_e^l [1 - (1 - S_e^{1/m})^m]^2 \tag{3}$$

where θ_r is the residual water content [$L^3 L^{-3}$], θ_s is the saturated water content [$L^3 L^{-3}$], α [L^{-1}], n [−] and m ($= 1 - 1/n$) [−] are shape parameters, l is the pore connectivity parameter [−], K_s is the saturated hydraulic conductivity [LT^{-1}], and $S_e = (\theta - \theta_r)/(\theta_s - \theta_r)$ is the effective saturation.

One-dimensional multicomponent transport in HP1 is described by means of aqueous master species (also called components or primary species), which reduces the number of transport equations to be solved. It is possible to write a given set of aqueous equilibrium reaction equations in terms of a limited set of independent master species or components (Morel and Hering, 1993):

$$\sum_{j=1}^{N_m} v_{ji} A_j^m = A_i \tag{4}$$

where N_m is the number of aqueous master species, $i = 1, ..., N_s$, N_s is the number of aqueous secondary species, A_j^m and A_i are the chemical equations for the master and secondary species, respectively, and v_{ji} are the stoichiometric coefficients in the reaction. The number of aqueous master species equals the total number of aqueous species minus the number of aqueous equilibrium reactions (if the reactions are written stoichiometrically independent). For each aqueous master component, solute transport is defined as (e.g., Lichtner, 1996; Mayer, 1999):

$$\frac{\partial \theta C_j}{\partial t} = \frac{\partial}{\partial x}\left(\theta D^w \frac{\partial C_j}{\partial x}\right) - \frac{\partial q C_j}{\partial x} - S C_{r,j} + R_{o,j} \tag{5}$$

where $j = 1, ..., N_m$, q is the volumetric flux density [LT^{-1}], S is the sink term in the flow equation (Eq. (1)), D^w is the dispersion coefficient in the liquid phase [$L^2 T^{-1}$], and C_j is the total liquid concentration of master species j [ML^{-3}]:

$$C_j = c_j + \sum_{i=1}^{N_s} v_{ji} c_i \tag{6}$$

Additionally, $C_{r,j}$ in Eq. (5) is the total concentration of the sink term (defined similarly as C_j), and $R_{o,j}$ is a reaction term that accounts for removal of a master species from the liquid phase due to aqueous kinetic reactions, and equilibrium or kinetic heterogeneous reactions [$ML^{-3}T^{-1}$] (e.g., sorption, ion exchange, mineral dissolution/precipitation). Kinetic reactions of virtually any form can be given by means of small BASIC programs in the input file, thus providing great flexibility for addressing a broad range of applications.

HP1 uses the operator-splitting approach without any iterations during a single time step (the non-iterative sequential approach). Among others, Walter et al. (1994) used this approach in a simple two-step procedure to couple physical and chemical processes. HP1 uses a more complex four-step approach (Fig. 1). Starting from the variables related to water flow (H^n, e.g., the pressure heads), heat
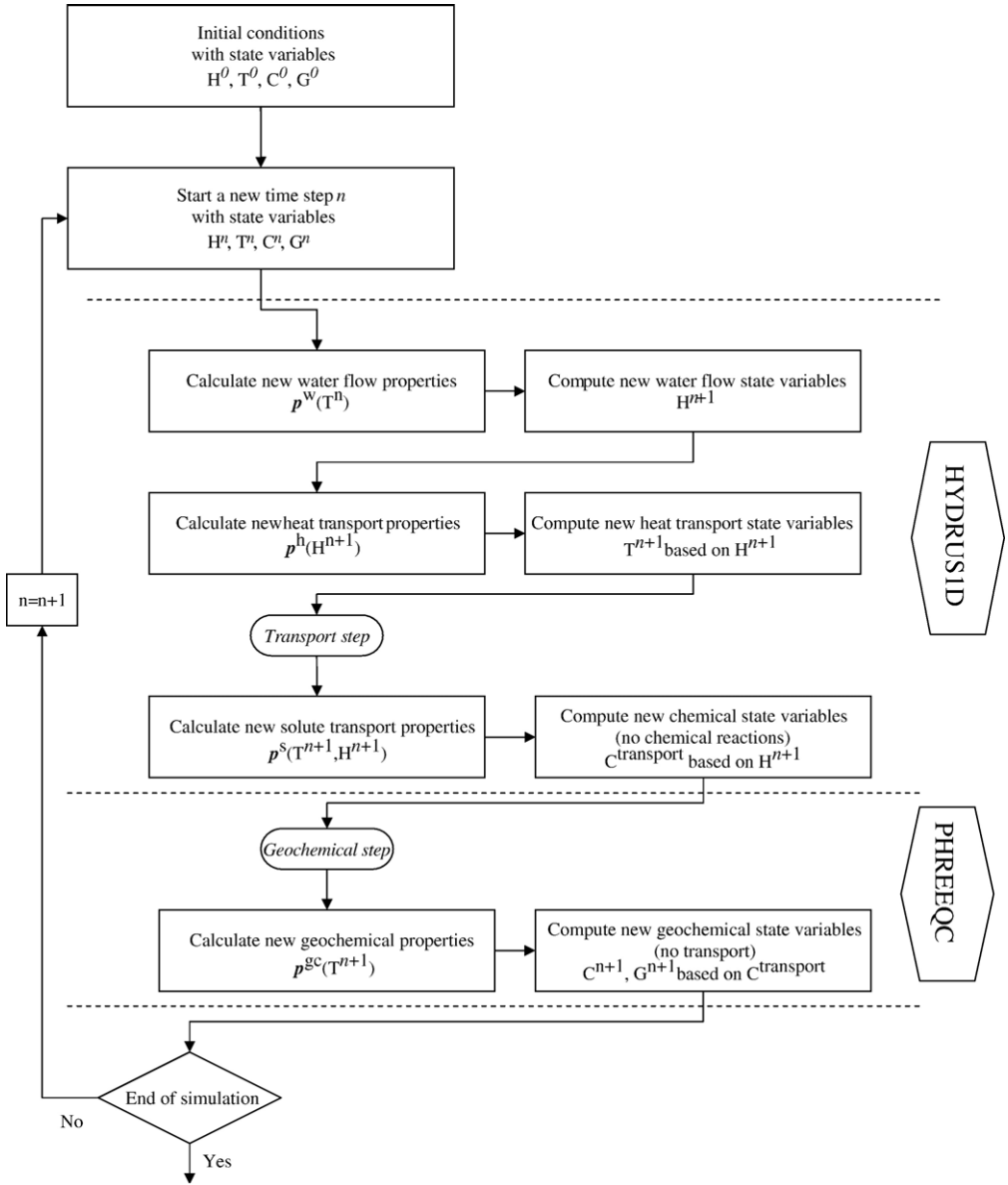
Fig. 1. Schematic flow chart of the operator-splitting approach used in HP1.

flow (T^n, e.g., temperatures), solute transport (C_j^n, e.g., the concentrations of master species j) and the solid phase (G^n, e.g., the mineralogical composition, exchange sites) at a given time step n, the sequence of solving the governing equation in the next time step Δt is:

(1) Calculate the new water flow properties $p^w(T^n)$ and solve the water flow Eq. (1) using H^n to obtain H^{n+1};

(2) Calculate the new heat transport properties $\boldsymbol{p}^h(H^{n+1})$ and solve the heat transport equation (Eq. 4.1 in Šimůnek et al., 1998; not further given here since only isothermal flow and transport problems are considered here) using H^{n+1} and T^n to obtain T^{n+1};

(3) Calculate the new solute transport properties $p^s(T^{n+1},H^{n+1})$ and solve the advection–dispersion equation for each master species j without any chemical reactions (Eq. (5) without the reaction term $R_{o,j}$; this source-sink term is solved in step 4 for all master species simultaneously) using H^{n+1} and C_j^n to obtain $C_j^{n,\text{phys}}$ (i.e., the transported concentrations without any chemical source or sink reactions). The advection–dispersion equation during each time step is solved N_m times (i.e., separately for each master species); and

(4) Calculate new geochemical properties $p^{\text{gc}}(T^{n+1})$ and solve the system of equations for geo-chemical speciation using $C_j^{n,\text{phys}}$ ($j=1, ..., N_m$) and G^n to obtain C_j^{n+1} (i.e., the concentrations at the end of the time step resulting from equilibrium and kinetic reactions) and G^{n+1}. This system is solved using the Newton–Raphson method for equilibrium reactions, together with the Runga–Kutta method for mixed equilibrium-kinetic reactions (see Parkhurst and Appelo, 1999). The first three steps are solved with the HYDRUS-1D part of HP1, which thus acts as the transport solver, whereas the PHREEQC part of HP1 is used for the fourth (geochemical) step.

A critical aspect of the solution scheme is optimal control of the time stepping process. Time stepping in HP1 is controlled by means of three criteria within the HYDRUS-1D transport solver. HYDRUS-1D has a self-adjusting time stepping scheme which changes the size of the time step depending upon the number of iterations needed to solve the Richards equation (Šimůnek et al., 1998). The time step, Δt, calculated in this manner is limited by two user-defined constraints: (i) the maximum allowed time step, and (2) the performance index ω_s (Perrochet and Berod, 1993), which is defined as the product of the grid Peclet number, Pe ($= q\Delta x/\theta D^w$) and the Courant number, Cr ($= q\Delta t/\theta\Delta x$). At the beginning of a new time step, the product of Pe and Cr is calculated for each grid cell using the updated Δt, but with q and θ from the previous time step. If the maximum value of this product is larger than the defined ω_s, Δt is decreased to fulfil the performance index requirement. Finally, Δt cannot be larger than a predefined maximum allowed time step, Δt. This means that for relatively high water fluxes, Δt is constrained mainly by ω_s, whereas the maximum allowed time step constrains Δt mostly during periods with low water fluxes. Šimůnek et al. (1998) suggested values less than 5 for Pe and less than 2 for ω_s (Perrochet and Berod, 1993) when using HYDRUS-1D separately from HP1.

2.2. Test criteria for numerical accuracy

The accuracy of the operator-splitting approach was assessed by comparing concentration profiles obtained with HP1 against concentration profiles obtained with codes that use a global implicit approach (which is considered here to give the correct reference solution). Errors will be quantified using the L_2 norm defined as (Steefel and MacQuarrie, 1996):

$$L_2 = \sqrt{\sum_{i=1}^{N_y} y_i^2} \tag{7}$$

where y is the vector of concentration differences $[\text{ML}^{-3}]$ between the HP1 results and the reference solution and N_y is the number of data points. Note that L_2 has the dimension of concentration, but this will not be further indicated in this paper. Depending upon the example problem discussed here, the reference solution is obtained by using (1) a global implicit approach that is implemented in

HYDRUS-1D for the transport of a first-order decay chain of adsorbing contaminants during transient variably saturated flow (example 1), and (2) a global implicit approach that is used in CRUNCH (Steefel, 2000) for the transport of major cations and heavy metals during steady-state flow in a soil profile having a pH-dependent cation exchange complex (example 2).

3. Results and discussion

3.1. Transport of a first-order decay chain of adsorbing contaminants during transient flow

3.1.1. Problem definition

This example considers the transport of three hypothetical contaminants (A_1, A_2, A_3) in a homogeneous soil profile covered with grass subject to atmospheric boundary conditions defined by a time series of precipitation P and potential evapotranspiration E_{TP} rates, and with free drainage as the lower boundary condition. The time series for P, potential evaporation E_p, and potential transpiration T_p were derived from climatological data for 3 years (1975–1977) from the Campaign region (Belgium) using a crop factor of 0.8 for grass (Vanclooster et al., 1994) and a time-variable leaf area index (see e.g. Hupet et al., 2002 for estimating E_p and T_p from E_{TP}). Fig. 2 shows the cumulative P, E_p, and T_p rates during the 3 year simulation period. Roots were assumed to be uniformly distributed within a 20-cm deep root zone, thus implying a constant potential root water uptake distribution in the root zone. The actual root water uptake rate may be lower due to soil moisture stress, which was described with the Feddes water uptake reduction model (Feddes et al., 1978; Table 1). The actual evaporation rate can similarly be lower than E_p when the hydraulic conductivity of the soil is too low to move enough water to the soil surface, thus causing a shortage of moisture near the soil surface. The actual evaporation rate was calculated from the potential evaporation rate by limiting the surface pressure head to the value determined from equilibrium conditions between soil water and atmospheric water vapour, and evaluating the actual surface flux for this limiting pressure head. Geochemical reactions involve both equilibrium (adsorption) and kinetic (first-order degradation) reactions. The adsorption reactions in this example were assumed to be linear for A_1 and nonlinear (Freundlich sorption) for A_2 and A_3. Degradation reactions were assumed to occur only in the liquid phase for A_1, but in both the liquid and solid phases for A_2 and A_3. Note that both the equilibrium adsorption and degradation reactions were solved with the
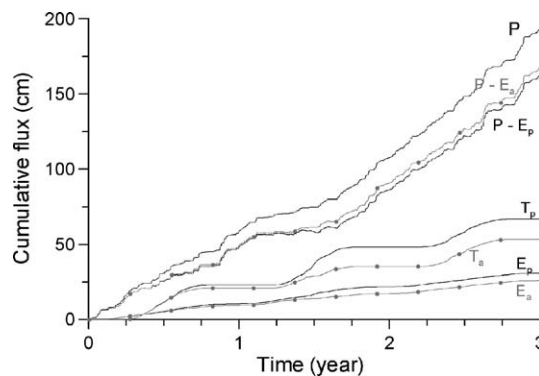

Fig. 2. Potential and simulated actual fluxes during three growing seasons (1975–1977) for the transport of a first-order decay chain of adsorbing contaminants. P — precipitation; E_p, E_a— potential and actual evaporation; respectively; T_p, T_a— potential and actual transpiration, respectively.

chemical solver of HP1 (i.e. PHREEQC), whereas inert transport was solved with the transport solver of HP1 (i.e., HYDRUS-1D). Table 1 lists the various hydraulic, solute transport, root water uptake and geochemical parameters of the assumed 1-m deep uniform medium-textured soil profile.

The numerical accuracy of the operator-splitting technique used in HP1 was assessed by comparisons against a numerical reference solution obtained with HYDRUS-1D. The reference solution was generated with a very small uniform spatial grid of 0.5 cm, a Peclet number of 0.5, and a maximum time step of 0.1 day. The maximum Courant number during the simulation was 0.197. The 0.5-cm discretization produced accurate water fluxes near the soil surface during both infiltration and evaporation (Van Dam and Feddes, 2000). The selected *Pe* and *Cr* values should also lead to a very accurate solution of the solute transport equation for this problem (Šimůnek et al., 1998).

Fig. 2 shows the cumulative actual transpiration rate (root water uptake) T_a, the cumulative actual evaporation rate E_a, and the cumulative actual surface flux $P-E_a$. Since the second growing season (year 1976) was very dry during summer, not enough soil water was available for potential transpiration and, to a lesser extent, for potential evaporation. Because of the transpiration reduction, the actual root water uptake rate hence was smaller than the potential root water uptake during this period. The smaller E_a produced a slightly larger cumulative actual surface flux compared to the

Table 1
Soil hydraulic, solute transport, root water uptake and geochemical parameters for simulating the transport of a first-order decay chain of adsorbing contaminants

Parameter	Symbol	Values	Unit
Soil hydraulic parameters[1]			
Saturated water content	θ_s	0.43	$cm^3\ cm^{-3}$
Residual water content	θ_r	0.078	$cm^3\ cm^{-3}$
Shape parameter	α	0.036	cm^{-1}
Shape parameter		1.56	–
Saturated hydraulic conductivity	K_s	24.96	$cm\ d^{-1}$
Solute transport parameters			
Bulk density	ρ_b	1.5	$g\ cm^{-3}$
Dispersivity	λ	1	cm
Root water uptake parameters			
Pressure head below which water uptake starts	P_0	−10	cm
Pressure head below which water uptake is maximal	P_{opt}	−25	cm
Pressure head below which water uptake is not more at its maximum	P_2	−1000	cm
Pressure head below which water uptake ceases	P_3	−8000	cm
Biogeochemical parameters			
Adsorption isotherm coefficient for A_1	K_{a1}	1	$cm^3\ g^{-1}$
Adsorption isotherm coefficient for A_2	K_{a2}	2.5	$cm^3\ g^{-1}$
Freundlich exponent for A_2	n_2	0.9	–
Adsorption isotherm coefficient for A_3	K_{a3}	5	$cm^3\ g^{-1}$
Freundlich exponent A_4	n_3	0.8	–
First-order degradation rate for A_1 in aqueous phase	k_{a1}	0.005	day^{-1}
First-order degradation rate for A_2 in aqueous phase	k_{a2}	0.06	day^{-1}
First-order degradation rate for A_3 in aqueous phase	k_{a3}	0.02	day^{-1}
First-order degradation rate for A_2 in solid phase	k_{s2}	0.006	day^{-1}
First-order degradation rate for A_3 in solid phase	k_{s3}	0.002	day^{-1}

[1]Parameters representative of a loamy soil (from Šimůnek et al., 1998).

potential surface flux. Note that differences between the potential and actual fluxes were almost negligible during the first and third growing seasons (years 1975 and 1977, respectively).

Prior to analyzing the accuracy of HP1, the effect of time stepping and discretization on inert solute transport was evaluated using HYDRUS-1D. We subsequently evaluated the accuracy of the HP1 results using three cases: (1) only equilibrium adsorption reactions; no degradation, (2) only degradation reactions; no sorption, and (3) mixed equilibrium sorption and kinetic degradation reactions.

3.1.2. Inert transport

This problem was simulated with HYDRUS-1D using three grid sizes ($\Delta x = 0.5$, 1, and 2 cm) assuming a maximum time step of 1 day, as well as with the reference solution scheme as discussed earlier (i.e., with $\Delta x = 0.5$ cm and a maximum $\Delta t = 0.1$ day). The L_2 norm for the simulated concentration profiles was calculated every 15 day. Fig. 3 shows L_2 values as a function of time. Larger grid sizes were found to produce larger values of L_2. Notice that L_2 varied considerably in time, with the largest values occurring during periods with high E_p, even when we used the same spatial discretization but a different maximum time step. During periods with high P, L_2 values were quite similar for the simulations with $\Delta x = 0.5$ cm and $\Delta x = 1$ cm (i.e., between 0.9 and 1.25 year and between 1.75 and 2.4 year). L_2 values decreased slightly when a smaller maximum time step was used (results not shown). The different spatial and time discretizations also produced differences in the water content and flux profiles (results not shown). Van Dam and Feddes (2000) showed that calculated evaporation rates sometimes change with increasing grid size, leading to errors in the water content and the fluxes. These errors in the flow field will induce numerical errors in the solute concentration, and hence may interfere with an accurate assessment of the operator-splitting errors discussed in the next sections. However, the concentration profiles obtained with the different grid sizes were consistent with each other and showed only limited enhanced numerical dispersion with increasing grid size.

Possible HP1 operator-splitting errors were quantified in terms of: (i) total $L_2 = (\sum L_2^2)^{0.5}$, (ii) wet L_2, being the same as total L_2 but limited to concentration profiles between 1.8 and 2.2 years (a relatively wet period with mainly infiltration), and (iii) max L_2. Wet L_2 was used to evaluate the accuracy of the sequential non-iterative approach when errors related to grid discretization are expected to be low.
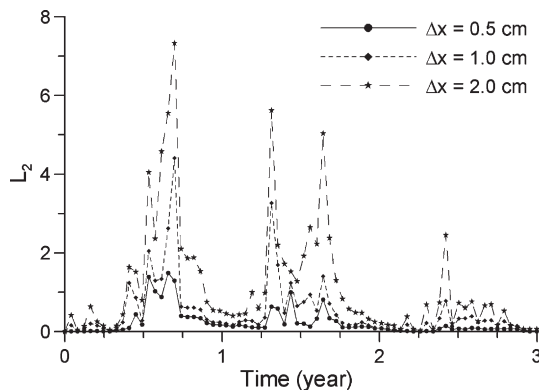

Fig. 3. Time series of L_2 values for the transport of an inert solute obtained with HYDRUS-1D for three grid sizes and a maximum time step of 1 day (reference solution is for $\Delta x = 0.5$ cm and a maximum time step of 0.1 day).

3.1.3. Transport subject to equilibrium adsorption

Next, the three contaminants were considered to undergo only equilibrium adsorption (linear for A_1, nonlinear for A_2 and A_3), but no kinetic degradation. No contaminants were assumed to be initially present and possible density effects after their application were neglected. Since no degradation took place (no degradation products from A_1), the concentration of each contaminant in the inflowing rain water was assumed to be simply 1 mol l^{-1} for all precipitation events. Simulations were carried out with different grid sizes, maximum time steps and varying performance indices ω_s (see Table 2). Fig. 4 shows total L_2, wet L_2, and max L_2 for A_1 and A_2 as a function of simulation time (A_3 concentrations were very similar to those of A_2, and are not further shown here). Results for the HYDRUS-1D simulations with different spatial discretizations and a maximum time step of 1 day are shown as straight lines. Note that while

Table 2
Overview of test simulations of the transport of the first-order solute decay chain

Run	Δx (cm)	Maximum time step (day)	ω_s	Simulation time (min)[a]		
				Only equilibrium reactions	Only kinetic reactions	Mixed equilibrium kinetic reactions
Reference case HYDRUS-1D						
	0.5	0.1	2	4.6	2.4	4.1
HYDRUS-1D runs						
a	2	1	2	0.8	0.5	0.7
b	1	1	2	1.5	1.0	1.4
c	0.5	1	2	3.1	2.1	1.3
HP1 runs						
1	2	1	1	16	82	76
2	2	1	0.5	22	84	78
3	2	1	0.25	19	94	85
4	2	0.25	0.25	20	104	108[b]
5	2	1	0.1	28	131	117
6	1	1	1	33	164	152
7	1	1	0.5	34	172	157
8	1	0.75	0.5	35	172	162
9	1	0.50	0.5	35	179	163[b]
10	1	0.25	0.5	38	195	205[b]
11	1	0.125	0.5	50	229	264[b]
12	1	1	0.25	38	187	171[b]
13	1	0.75	0.25	38	189	172
14	1	0.50	0.25	38	190	173
15	1	0.25	0.25	40	202	187
16	1	0.125	0.25	51	235	237[b]
17	1	1	0.1	60	275	269
18	0.5	1	1	73	377	382
19	0.5	1	0.5	73	378	385
20	0.5	1	0.25	80	417	422[b]
21	0.5	0.25	0.25	86	391	507
22	0.5	1	0.1	116	526	598[b]

[a] On a Pentium(R) 4, 3.06 GHz.

[b] These runs did not finish in one time, but were restarted from the last saved information before failure. All runs finished using this two-step approach. Hypothetical time the simulation would need if completed in one run; value was calculated based on the number of time steps multiplied by the average computational time needed for one time step during the first part of the simulation.
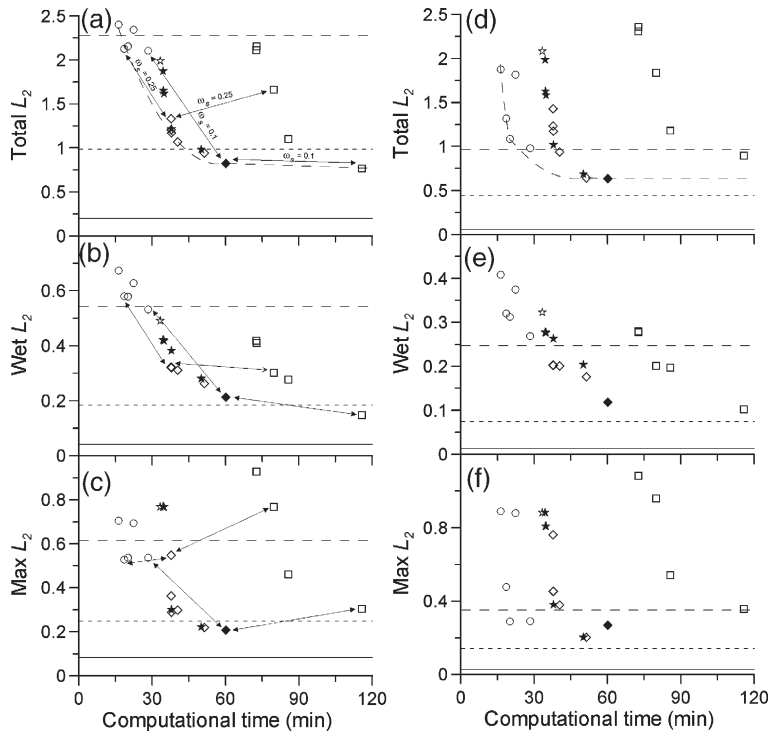
Fig. 4. L_2 measures for simulations of the transport of adsorbing contaminants (only equilibrium reactions) for A_1 (a–c) and A_2 (d–e) (square: $\Delta x = 0.5$ cm; open star: $\Delta x = 1$ cm, $\omega_s = 1$; solid star: $\Delta x = 1$ cm, $\omega_s = 0.5$; open diamond: $\Delta x = 1$ cm, $\omega_s = 0.25$; solid diamond: $\Delta x = 1$ cm, $\omega_s = 0.1$; open circle: $\Delta x = 2$ cm). Also shown are HYDRUS-1D results for $\Delta x = 0.5$ cm (solid lines), $\Delta x = 1$ cm (short dashed lines), and $\Delta x = 2$ cm (long dashed black lines). The long curved dashed grey lines in (a) and (d) are indicative of Pareto fronts.

we did not identify every simulation separately in Fig. 4, the smaller ω_s or the maximum time step, the smaller generally the accuracy measures. Using the computational times listed in Table 2, it is possible to identify the individual simulation runs as needed.

Contaminant A_1 was found to be the most mobile, and A_3 the least (results again not shown for the latter). Errors associated with the HYDRUS-1D grid discretization were found to be positively correlated with the mobility of the contaminants: largest for A_1 and smallest for A_3. There are several reasons for this: (1) since the more mobile solutes travelled deeper in the soil profile compared to the less mobile solutes, more non-zero terms are included in L_2, (2) due to the higher sorption, concentrations in the liquid phase are smaller for the less mobile solutes, thus making L_2 smaller, and (3) errors in the fluxes for larger grid sizes have less impact on the transport of the less mobile solutes. By comparison, the less mobile contaminants produced larger errors for the operator-splitting scheme relative to the grid discretization errors of HYDRUS-1D. HP1 simulations with $\Delta x = 1$ or 2 cm reached the total L_2 value for the HYDRUS-1D simulation for A_1, but not with $\Delta x = 1$ cm for A_2. The HP1 simulations with $\Delta x = 0.5$ always produced larger total L_2 values as compared to HYDRUS-1D (run c). These results suggest that operator-splitting errors during transient flow may increase with decreasing grid size (as opposed to grid discretization errors as evaluated with HYDRUS-1D) and decreasing mobility (or increasing nonlinearity for small grid sizes).

We now focus on the HP1 simulations (symbols in Fig. 4) in order to provide insight in the operator-splitting errors, and to identify possible strategies for maximizing accuracy with only a limited increase in computational time. Values of total L_2 for A_1 for $\Delta x = 1$ and $\Delta x = 0.5$ cm were quite similar. This suggests that the same level of accuracy can be obtained with a coarser grid ($\Delta x = 1$ cm with adjusted ω_s value and maximum time step) and with less computational time as compared to the finer grid ($\Delta x = 0.5$ cm). Even coarser grids could be used for the less mobile nonlinearly adsorbing contaminants (A_2 and A_3), which would lead to significantly smaller computational times (Table 2).

A comparison of wet L_2 and max L_2 reveals several other aspects of the accuracy of HP1 for transient flow problems. As a reference, lines (with arrows) connect simulations with the same maximum time step (1 day) and ω_s (but for different Δx): $\omega_s = 0.25$ (circle, open diamond and square for $\Delta x = 2$, 1, and 0.5 cm, respectively) and $\omega_s = 0.1$ (circle, solid diamond and square for $\Delta x = 2$, 1, and 0.5 cm, respectively). Simulations with $\Delta x = 0.5$ cm performed better than the coarser grid sizes during the main infiltration periods for a given combination of ω_s and maximum time step (wet L_2 in Fig. 4). On the other hand, the fine discretization produced a larger max L_2, especially for larger ω_s values. As was the case with the HYDRUS-1D runs, the max L_2 occurred during high E_p boundary conditions (Fig. 3 for the HYDRUS-1D simulations). The increases in max L_2 for A_1 when Δx decreased from 1 to 0.5 cm were 40 (i.e., from 0.5488 to 0.7687) and 46% (i.e., from 0.2076 to 0.3039) for ω_s 0.25 and 0.1, respectively. However, since errors are smaller for the finer grid during wet boundary conditions, total L_2 was only 25% larger for the finer grid when $\omega_s = 0.25$, whereas the total L_2 is similar when $\omega_s = 0.1$. The max L_2 decreased significantly when we used smaller ω_s values ($\Delta x = 0.5$ cm) or a combination of smaller maximum time steps and ω_s values ($\Delta x = 1$ cm). For the less mobile nonlinearly adsorbing contaminants (A_2 and A_3), smaller ω_s values for the simulations with $\Delta x = 0.5$ cm did not produce smaller max L_2-values than those obtained with the coarsest discretization, as was the case for A_1.

The simulations with $\Delta x = 1$ cm allow us to identify how operator-splitting errors can be reduced in a computationally efficient way by adjusting the maximum time step and/or ω_s. Wet L_2 can be reduced most efficiently by reducing ω_s. Decreasing ω_s from 1 to 0.25 (with a maximum time step of 1 day) produced significantly lower wet L_2 values without a significant increase in computational effort. On the other hand, decreasing the maximum time step resulted in a significant decrease in max L_2, with a negligible increase in simulation time (maximum time steps of 1, 0.75, 0.5 and 0.25 for $\omega_s = 0.5$ and 0.25). This was to be expected since wet L_2 was calculated during a period with high infiltration rates, a wet soil profile, and high water fluxes, and thus likely high Courant numbers. The performance index ω_s determines the maximum allowed Cr (for a fixed Pe) and thus the time step. Reducing ω_s hence leads to smaller time steps when water fluxes are high. As discussed earlier, max L_2 occurs during periods with high E_p (and low precipitation), and hence when the water fluxes in the soil are relatively small. The time step is then not controlled by ω_s, but by the maximum time step. Decreasing the latter thus should have its largest effect on L_2 during dry periods.

The plots in Fig. 4 can be interpreted also in terms of a multi-objective optimization with accuracy (as estimated with the different L_2 measures) and computational time as the two objectives. The grey dashed lines in Fig. 4a and d show so-called Pareto fronts (Stadler, 1988). Sharp Pareto fronts for all contaminants indicate that the accuracy can be significantly improved with minor increases in computational time. However, further improvement in accuracy beyond a given level may require considerably more computational time. Several non-Pareto optimal runs appear to exist, including 4 of the 5 runs for $\Delta x = 0.5$, some runs for $\Delta x = 1$ cm for A_1, and many runs for $\Delta x = 1$ cm for A_2.

Relatively good accuracy for all contaminants may be obtained by using a grid discretization of 1 cm, $\omega_s = 0.25$, and maximum time steps of 0.25 day resulting in a computational time of
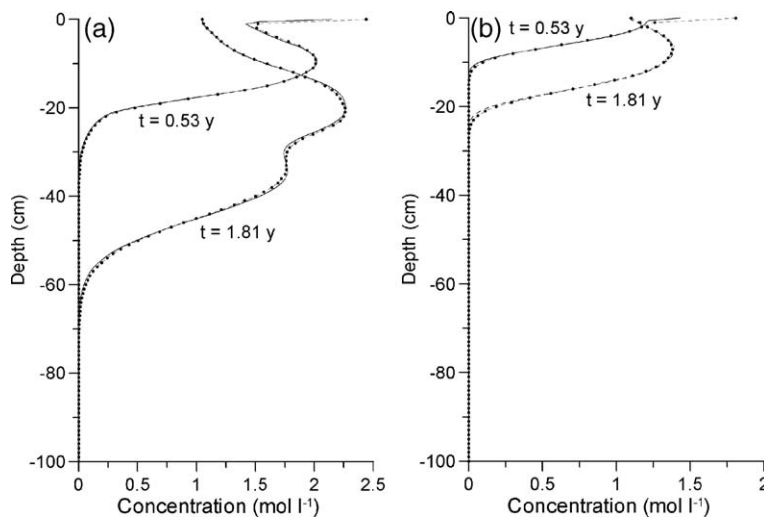
Fig. 5. Concentration profiles of A_1 (a) and A_2 (b) for the transport of adsorbing contaminants (only equilibrium reactions) for the reference case (black lines) and run 15 (grey lines with dots) at $t=0.53$ year and $t=1.81$ years. These times correspond to the time with max L_2 and the largest L_2-value during the wet period (between 1.8 and 2.2 years).

40 min. The accuracy could be further improved slightly by reducing the maximum time step to 0.125 day, which would increase the computational time by 10 min. While this increase may seem relatively small, the computational time would increase to 60 min when the equilibrium reactions are combined with the kinetic degradation reactions (to be discussed later, and shown in Table 2).

Fig. 5 shows concentration profiles for A_1 and A_2 for the max L_2 value and the highest L_2 value during the 'wet' period. Differences between the reference case and run 15 (Table 2) were very small. The largest difference occurred at the soil surface when E_p was large.

3.1.4. Transport subject to kinetic degradation

The same runs as in the previous example were carried out for a problem involving only kinetic degradation reactions (using parameters as defined in Table 1). Computational times were much
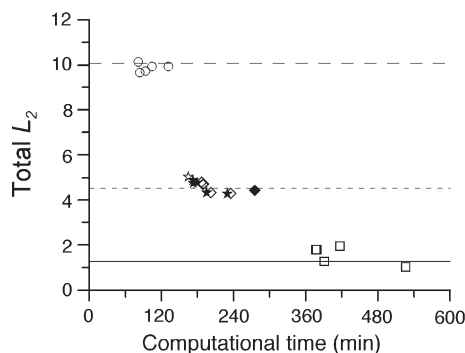

Fig. 6. Total L_2 for simulations of the transport of a first-order decay chain of three contaminants (only kinetic reactions) for A_1. Symbols are explained in Fig. 4.
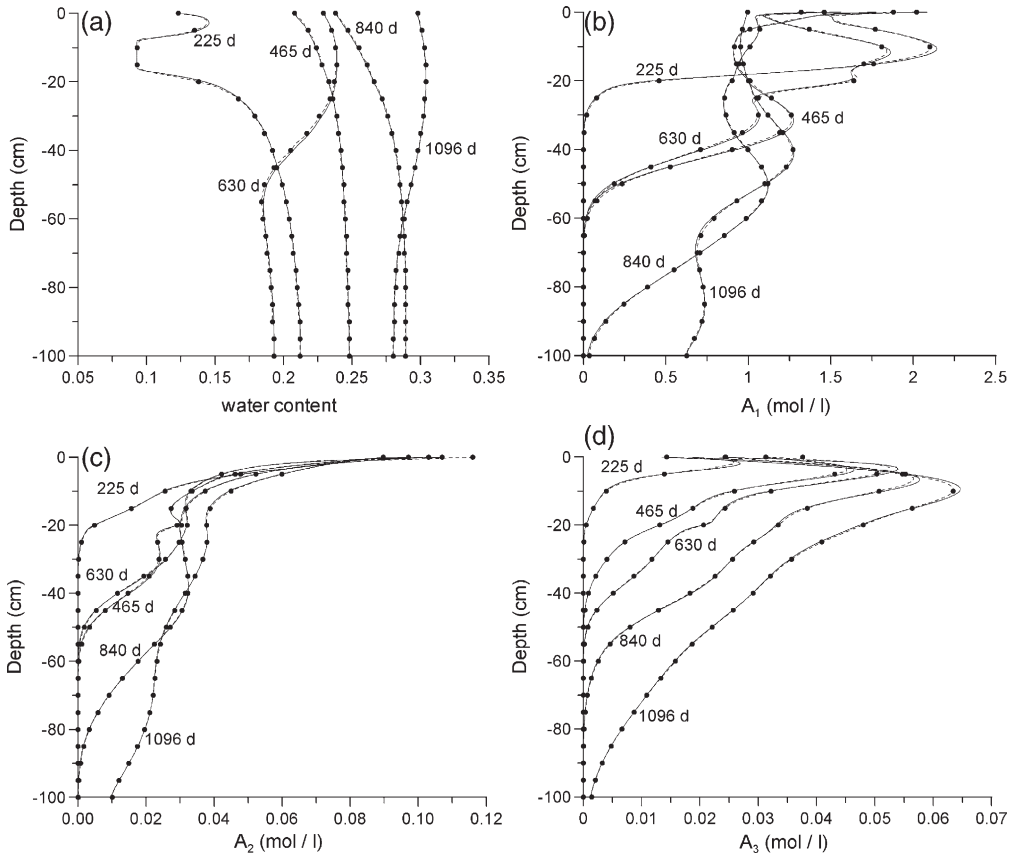
Fig. 7. Water content and concentration profiles at selected times for the transport of a first-order decay chain of adsorbing contaminants obtained with the reference run (black lines) and run 15 (grey lines with dots).

larger than those needed for the runs with only equilibrium reactions. Since kinetic reactions in PHREEQC are solved using the Runga–Kutta technique, the computational time for solving the geochemical part of the problem was much larger than when only equilibrium reactions are present. Optimizing the grid size and time steps is hence much more important when kinetic reactions are involved.

Table 3
Soil hydraulic properties and cation exchange capacities of the five soil horizons of the hypothetical sandy soil used for test example 1

Horizon	Layer thickness (cm)	θ_r	θ_s	α (cm^{-1})	n	K_s (cm day^{-1})	l	Cation exchange capacity (eq/1000 cm^3 soil)
A	13	0.065	0.476	0.016	1.94	93	0.5	0.0183
E	10	0.035	0.416	0.015	3.21	311	0.5	0.0114
Bh1	5	0.042	0.472	0.016	1.52	39	0.5	0.0664
Bh2	5	0.044	0.455	0.028	2.01	860	0.5	0.0542
Bh/C	17	0.039	0.464	0.023	2.99	1198	0.5	0.0116

Table 4
Hypothetical pH and solution concentrations of the initial soil solution and the infiltrating solution (μmol l^{-1}) for example 2

Solution	pH	Na*	K	Ca	Mg	Br	Cd	Pb	Zn
0–28 cm depth	8.5	401.9	120	98	5	780	0.8	2.5	50
28–50 cm depth	8.5	454.0	120	98	5	780	0.0	0	0
Applied water	3.5	127.5	120	98	5	780	0.0	0	0

* Concentration of Na was adjusted to obtain the desired pH.

Fig. 6 shows the total L_2 for A_1 for different runs. Results for the other L_2 measures and the other two contaminants were very similar and are not shown here. Notice that the L_2 values are larger than those for the simulations with only equilibrium adsorption reactions (Fig. 4). When only kinetic degradation occurs and no sorption, the contaminants are more mobile, leading to larger errors for the coarser spatial discretizations (see discussion in Section 3.1.3.), with the errors becoming of the same magnitude as for the inert tracer simulations (Section 3.1.2, Fig. 3).

HP1 errors were close to those obtained with HYDRUS-1D for different grid discretizations, indicating that operator-splitting errors are small. This is due to the fact that the first-order degradation constants are small relative to the time steps. Carrayrou et al. (2004) showed that when the dimensionless time N_{OS1} ($=k\Delta t$ with k the first-order degradation constant) is smaller than 0.1, mass balance errors will be less than 1%, also for the non-iterative operator-splitting approach. For a maximum time step of 1 day, N_{OS1} in our example was less than 0.1, which should lead to relatively small mass balance errors. Also, the time steps were generally smaller than the maximum time step for the transient flow simulations, thus leading to even smaller errors.

3.1.5. Transport subject to combined equilibrium adsorption and degradation

This last step of our analysis considers a combination of equilibrium adsorption and kinetic degradation using the full set of parameters defined in Table 1. Not all runs finished the 3 years simulation in one time, notably those for $\Delta x = 0.5$ cm, and those with a maximum time step of 0.125 day or $\omega_s = 0.1$ for $\Delta x = 1$ cm (the reason for this failure was not clear since no convergence error in PHREEQC occurred). Each run, however, could be finished when it was restarted from the latest save of the profile information. The various accuracy measures were limited to only the first 1.8 year (i.e., shortest run), while wet L_2 was calculated between 0.74 and 1.11 years. Table 2 lists

Table 5
Overview of aqueous equilibrium reactions and corresponding equilibrium constants for example 2 (data from the phreeqc. dat database, Parkhurst and Appelo, 1999)

Nr	Aqueous speciation reaction	Log_K		
(1)	$H_2O = OH^- + H^+$	-14		
(2)	$Na^+ + H_2O = NaOH + H^+$	-14.18		
(3)	$K^+ + H_2O = KOH + H^+$	-14.46		
(4)	$Ca^{2+} + H_2O = CaOH^+ + H^+$	-12.78		
(5)	$Mg^{2+} + H_2O = MgOH^+ + H^+$	-11.44		
		Cd	Pb	Zn
(6)	$Me^{2+} + H_2O = MeOH^+ + H^+$	-10.08	-7.71	-8.96
(7)	$Me^{2+} + 2H_2O = Me(OH)_2 + 2\ H^+$	-20.35	-17.12	-16.90
(8)	$Me^{2+} + 3H_2O = Me(OH)_3^- + 3\ H^+$	-33.30	-28.06	-28.40
(9)	$Me^{2+} + 4H_2O = Me(OH)_4^{2-} + 4\ H^+$	-47.35	-39.70	-41.20

Table 6
Log K parameters for the multi-site exchange complex used in example 2

Y-exchanger [a]	NaY	KY	MgY$_2$	CaY$_2$	CdY$_2$	PbY$_2$	ZnY$_2$
	−1.0	−0.3	−0.4	−0.2	−0.2	0.05	−0.2
HY[b]	HYa	HYb	HYc	HYd	HYe	HYf	
	1.65	3.3	4.95	6.85	9.6	12.35	

  [a] The value for NaY was taken from Appelo et al. (1998). Values for the other complexes were taken from the phreeqc.
dat database (Parkhurst and Appelo, 1999) and adapted relative to the K for NaY.
  [b] Values taken from Appelo et al. (1998).

computational times for those runs that finished normally, as well as extrapolated computational times for those that were terminated early. The computational times were similar to those obtained for the kinetic reactions alone.

Although the L_2 measures were calculated for a different time period, similar Pareto fronts were observed as for simulations with only equilibrium reactions (results not shown). Again, a good compromise between required computational time and accuracy was obtained with $\Delta x = 1$ cm, $\omega_s = 0.25$, and a maximum time step of 0.25 day. It is important to note that the wet L_2 for $\Delta x = 0.5$ cm and $\omega_s = 0.1$ also resulted in the lowest value for all runs.

The water content and concentration profiles at selected times for run 15 were found to be in good agreement with the reference HYDRUS-1D simulations (Fig. 7). In general, errors associated with both operator-splitting and grid discretization were relatively small, leading to accurate results for HP1. Notice that the effects of root water uptake are clearly visible in Fig. 7 by the lower water contents in the top 20 cm of the profile at $t = 225$ day.

3.2. Heavy metal transport with a pH-dependent cation exchange complex

In order to describe the competition between protons, major cations and heavy metals for adsorption sites as a function of pH, Appelo et al. (1998) previously proposed a multi-site cation exchange complex consisting of several sites, each having a different selectivity coefficient for the exchange of protons. Their model captures the typical behaviour and increased capacity of the surfaces to adsorb major cations and heavy metals at higher pH values. The model for cation exchange in the presence of organic matter and Fe-oxyhydroxides consists of six sites. The multi-site cation exchange complex model was used in the second test example to simulate the transport of several major cations (Na, K, Ca, and Mg) and three heavy metals (Cd, Zn, and Pb) in a heavy-metal

Table 7
Overview of test simulations of the transport of heavy metals with a pH-dependent cation exchange complex

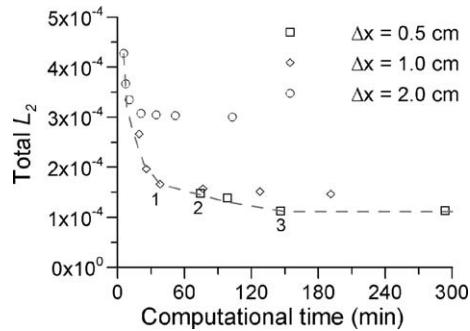| $\Delta x = 0.5$ cm		$\Delta x = 1$ cm		$\Delta x = 2$ cm	
Maximum time step (day)	ω_s	Maximum time step (day)	ω_s	Maximum time step (day)	ω_s
0.0145	0.1	0.0290	0.2	0.0579	0.4
0.0108	0.075	0.217	0.15	0.0434	0.3
0.0073	0.05	0.0146	0.1	0.0292	0.2
0.0036	0.025	0.0072	0.05	0.0145	0.1
		0.0043	0.03	0.0087	0.06
		0.0029	0.02	0.0058	0.04
				0.0029	0.02

Fig. 8. Total L_2 summed over 7 cations for simulations of the transport of major cations and heavy metals in a soil with a pH-dependent cation exchange complex during steady-state flow. The grey dashed line indicates the Pareto front. Numbers indicate Pareto optimal runs shown in Fig. 9.

contaminated soil that initially had a high pH (8.5), but was subjected to infiltration with an acid heavy-metal-free solution (pH 3).

The 60-cm deep soil profile was assumed to contain five distinct soil horizons with different soil hydraulic properties and exchange capacities (Table 3). The reported CEC is the sum of the CEC of the six sites, with each site having the same CEC. A constant water flux of 0.05 m day^{-1} and free drainage were taken as the upper and lower boundary conditions, respectively. This situation leads to unsaturated flow with the water content varying with depth. We used a dispersivity of 0.05 m and a diffusion coefficient of $9.2 \cdot 10^{-10}$ m^2 s^{-1}. Table 4 lists the concentrations of the initial soil solution and the infiltrating solution. Note that only the top 30 cm of the soil profile was initially contaminated with the three heavy metals. The considered aqueous equilibrium reactions (with their corresponding equilibrium constants) and the parameters for the multi-site exchange complex are given in Tables 5 and 6, respectively. The six sites are identified in Table 6 as Ya, Yb, …, Yf, with equilibrium constants for the same element (Na, K, Mg, Ca, Cd, Pb and Zn) being identical (first two rows in Table 6, where Y is understood to refer to Ya, …, Yf). The sites all have different equilibrium constants for the exchange of the protons, as shown by the third and fourth rows in Table 6.

HP1 simulations in terms of L_2 will be compared with results obtained with CRUNCH (Steefel, 2000), which solves the problem using a global implicit approach and therefore is considered to be the reference run. The reference run used a spatial discretization $\Delta x = 0.5$ cm and a maximum time step of 0.055 day. HP1 simulations were performed for three spatial discretizations ($\Delta x = 0.5$, 1, and 2 cm) and for different maximum time steps (d) with corresponding ω_s-values (Table 7). L_2 values were calculated for the concentration profiles of each component for every 5 days between day 0 and day 365.

Fig. 8 shows a plot of the total L_2 ($=(\sum L_2^2)^{0.5}$) for all 7 cations combined (Na, K, Ca, Mg, Cd, Pb, Zn) versus the required computer time (for a Pentium 4 3.06 GHz computer). Different simulations for a given Δx can be identified by the longer computational time for smaller ω_s values. For steady-state flow conditions, a finer spatial discretization produced a smaller L_2 norm. This is in contrast to the transient flow simulations which showed slightly larger L_2 norms with finer grids (see Section 3.1.2), but similar to the wet L_2 norm defined in Section 3.1.2 (only equilibrium reactions). Neglecting periods with high evapotranspiration (as was done for the wet L_2 norm), the finer discretizations produce more accurate results. For the steady-state flow situations considered here, this effect was very clear. The coarser grid sizes never reached the accuracy of the smaller grid sizes, even after reducing the maximum time step for the coarser

grids. However, the difference between $\Delta x = 2$ cm and $\Delta x = 1$ cm was much larger than the difference between $\Delta x = 1$ and $\Delta x = 0.5$ cm.

A Pareto front drawn through the data in Fig. 8 shows the non-optimal runs. Cd outflow curves and profiles of Ca, Cd and pH for three Pareto front runs ($\Delta x = 1$ cm, $\omega_s = 0.05$; $\Delta x = 0.5$ cm, $\omega_s = 0.1$ and 0.05) are shown in Fig. 9 together with the reference run using CRUNCH. Infiltration with the low-pH solution causes a decrease in the capacity of the solid surfaces to adsorb heavy metals in favour of protons. This will lead to desorption of heavy metals and subsequent leaching from the soil profile (Fig. 9a, showing leaching of Cd).

3.3. Strategy for reducing operator-splitting errors

The spatial and time discretizations suggested earlier hold only for the specific combination of soil, time series of ET_p and P, and the particular geochemical properties of the contaminants used in our examples. A more elaborate analysis covering a range of contaminant properties, soil types, and infiltration and evapotranspiration rates is required to provide more general guidelines. Still, our analyses indicates that (i) operator-splitting errors are small for kinetic reactions when the kinetic
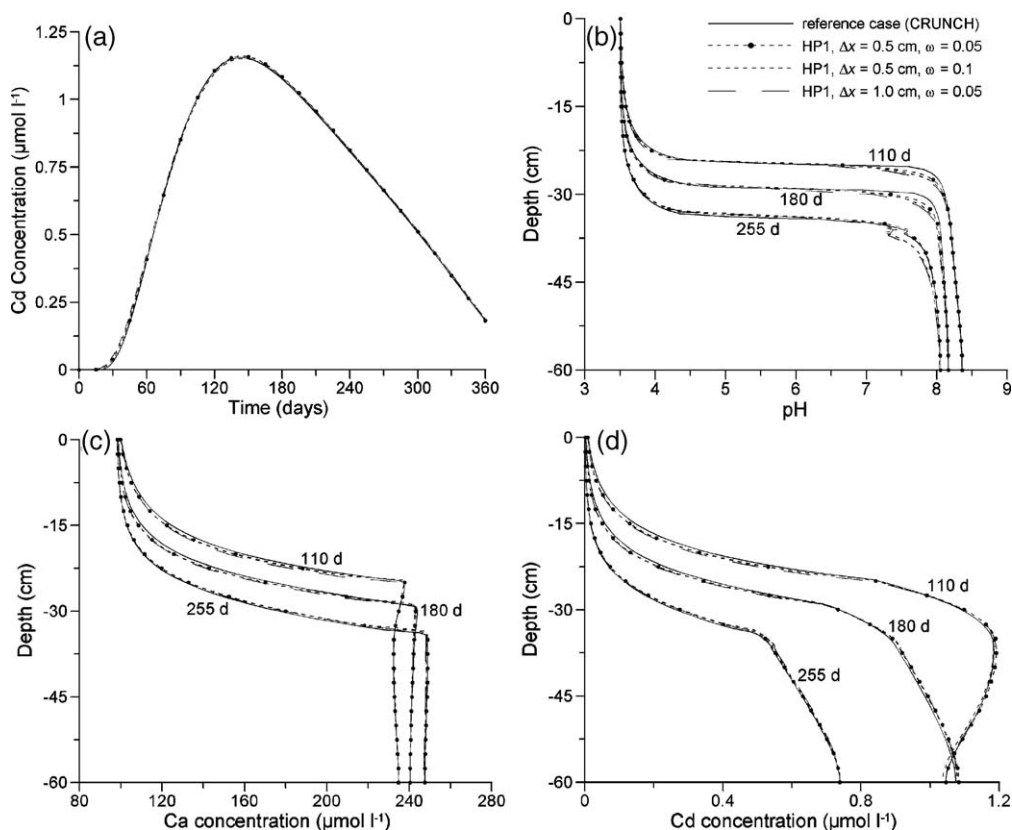

Fig. 9. Calculated Cd outflow curves (a) and profiles of pH (b), Ca concentrations (c) and Cd concentrations (d) for the transport of major cations and heavy metals in a soil with a pH-dependent cation exchange complex during steady-state flow. HP1 ($\Delta x = 0.5$ cm, $\omega_s = 0.05$), HP1 ($\Delta x = 0.5$ cm, $\omega_s = 0.1$), and HP1 ($\Delta x = 1.0$ cm, $\omega_s = 0.05$) correspond to the Pareto optimal runs 1, 2, and 3 indicated in Fig. 8.

rates are small relative to the time steps. Given that time steps during transient flow simulations are small, operator-splitting errors can be easily controlled for these type of problems; (ii) in case of equilibrium heterogeneous reactions (linear and nonlinear sorption and cation exchange studied here), numerical errors are reduced by reducing the grid size for steady-state flow conditions or during wet periods with mainly infiltration; and (iii) during transient flow (especially during periods with mainly evaporation), operator-splitting errors depend in a complex manner on the grid discretization and the time stepping. In that case, the finest grid discretization with the smallest ω_s value and maximum time step will lead to the smallest wet L_2 value. Our simulation results hence may serve as a preliminary guide for selecting a reasonable spatial and temporal discretization.

In view of our simulations we suggest the following procedure for selecting time step constraints for other problems: (1) select a short period from a time series of P and ET_p containing both wet and dry periods with high ET_p (e.g., 2 years out a 30-year simulation period) or one simulation out of a set of many (e.g., in uncertainty analyses), (2) run the model with a relatively fine grid, low ω_s and a small maximum time step to obtain a reference solution (which may require a long computational time), (3) run the model for several cases with coarser grids and a larger ω_s, (4) calculate wet L_2 using the reference run to analyze the effect of grid discretization and ω_s, and determine an optimal Δx, (5) run the model for several cases with larger maximum time steps for a fixed (optimum) grid discretization and possibly also a fixed ω_s, and (6) calculate max L_2 using the case with the smallest maximum time step as reference for a fixed grid discretization to analyze the effect of the maximum time step on the error.

4. Conclusions

A non-iterative sequential coupling approach may be used to combine separate water flow and solute transport codes with geochemical speciation codes. Although such coupling has many advantages from a programmer's perspective, its most important disadvantage is the possible occurrence of operator-splitting errors. This paper investigates several ways to reduce these type of errors in transient flow problems by optimizing grid discretization and time stepping, the latter in terms of two controlling parameters: the maximum time step and the performance index ω_s.

The most critical system we investigated involved heterogeneous equilibrium reactions during transient flow conditions (example 1). Contrary to the global-implicit approach, we found that finer spatial discretizations do not always lead to smaller numerical errors, especially for less mobile solutes with fine grids during dry periods with a high evapotranspiration demand. This result is in contrast with steady-state flow problems where finer grids did produce smaller operator-splitting errors. Also, for (relatively slow) kinetic reactions, coarser grids introduced larger numerical errors for transient flow situations, but results were independent of the operator-splitting errors due to the small values of the dimensionless rate constant N_{OS1} (smaller than 0.1, Carrayrou et al., 2004). We note here that time steps during transient variably-saturated flow simulations often are already relatively small to enable accuracy in solutions of the flow equation, thus frequently ensuring small N_{OS1} values. The observation that numerical errors are in some cases larger during transient flow simulations when finer grids are used indicates that operator-splitting errors are more significant during periods with high E_p boundary conditions with finer grids.

Adequate time step control is required for transient flow simulations when using a reactive coupled code. An optimal combination of the two criteria determining the time steps (maximum time step and ω_s) is critical. To reduce numerical errors during periods of infiltration, ω_s is the most appropriate and efficient parameter. The maximum time step is the more important factor determining numerical errors during time periods with high evapotranspiration rates.

Since our analysis was carried out for only one soil type and a limited number of contaminants with different adsorption properties, results should not be used to provide general guidelines for optimal choice of the performance index and the maximum time step. Following the procedures used in this paper, a fine spatial grid discretization (e.g., $\Delta x = 0.5$ cm) could be used in combination with a small ω_s value (e.g., 0.125) and a small maximum time step (e.g., 0.125 day depending on the total simulation time and water fluxes) to first generate an accurate numerical solution during infiltration events at high computational cost. This reference solution could then be used to test the accuracy of alternative spatial and time discretizations for a particular problem at a lower computational cost, but with increased accuracy during periods of high evapotranspiration.

Acknowledgements

References

Adler, M., 2001. Interaction of claystone and hyperalkaline solutions at 30 °C: A combined experimental and modeling study. Ph. D., Universitaet Bern, 120 p.

Appelo, C.A.J., Verweij, E., Schäfer, H., 1998. A hydrogeochemical transport model for an oxidation experiment with pyrite/calcite/exchangers/organic matter containing sand. Appl. Geochem. 13, 257–268.

Ayora, C., Taberner, C., Saaltink, M.W., Carrera, J., 1998. The genesis of dedolomites: a discussion based on reactive transport modeling. J. Hydrol. 209, 346–365.

Barry, D.A., Miller, C.T., Culligan-Hensley, P.J., 1996. Temporal discretisation errors in non-iterative split-operator approaches to solving chemical reaction/groundwater transport models. J. Contam. Hydrol. 22, 1–17.

Barry, D.A., Miller, C.T., Culligan, P.J., Bajracharya, K., 1997. Analysis of split operator methods for nonlinear and multispecies groundwater chemical transport models. Math. Comput. Simul. 43, 331–341.

Carrayrou, J., Mosé, R., Behra, P., 2004. Operator-splitting procedures for reactive transport and comparison of mass balance errors. J. Contam. Hydrol. 68, 239–268.

Davis, J.A., Meece, D.E., Kohler, M., Curtis, G.P., 2004. Approaches to surface complexation modeling of Uranium(VI) adsorption on aquifer sediments. Geochim. Cosmochim. Acta 68, 3621–3641.

Feddes, R.A., Kowalik, P.J., Zaradny, H., 1978. Simulation of field water use and crop yield. John Wiley and Sons, New York, NY.

Hundsdorfer, W., Verwer, J.G., 1995. A note on splitting errors for advection-reaction equations. Appl. Numer. Math. 18, 191–199.

Hupet, F., Lambot, S., Javaux, M., Vanclooster, M., 2002. On the identification of macroscopic root water uptake parameters from soil water content observations. Water Resour. Res. 38, 1300, doi:10.1029/2002WR001556.

Jacques, D., Šimůnek, J., 2005. User manual of the multicomponent variably-saturated flow and transport model HP1: Description, Verification, and Examples (Version 1.0). SCK•CEN, Mol, Belgium, BLG-998, 79 p.

Kaluarachchi, J.J., Morshed, J., 1995. Critical assessment of the operator-splitting technique in solving the advection–dispersion-reaction equation: 1. First-order reaction. Adv. Water Resour. 18, 89–100.

Kent, D.B., Abrams, R.H., Davis, J.A., Coston, J.A., LeBlanc, D.R., 2000. Modelling the influence of variable pH on the transport of zinc in a contaminated aquifer using semi-empirical surface complexation models. Water Resour. Res. 36, 3411–3425.

Kohler, M., Curtis, G.P., Kent, D.B., Davis, J.A., 1996. Experimental investigation and modeling of uranium(VI) transport under variable chemical conditions. Water Resour. Res. 32, 3539–3551.

Langergraber, G., Šimůnek, J., 2005. Modeling variably-saturated water flow and multicomponent reactive transport in constructed wetlands. Vadose Zone J. 4, 924–938.

Lichtner, P.C., 1996. Continuum formulation of multicomponent–multiphase reactive transport. In: Lichtner, P.C., Steefel, C.I., Oelkers, E.H. (Eds.), Reactive transport in porous media. Reviews in Mineralogy, vol. 34. Mineralogical Society of America, Washington, DC, pp. 1–81.

Mayer, K.U., 1999. A numerical model for multicomponent reactive transport in variably saturated porous media. Ph.D. thesis, Department of Earth Sciences, University of Waterloo, 285 p.

Mayer, K.U., Frind, E.O., Blowes, D.W., 2002. Multicomponent reactive transport modeling in variably saturated media using a generalized formulation for kinetically controlled reactions. Water Resour. Res., doi:10.1029/2001WR000682.

Meeussen, J.C., Scheidegger, A., Hiemstra, T., van Riemsdijk, W.H., Borkovec, M., 1998. Predicting multicomponent adsorption and transport of fluoride at variable pH in a goethite–silica sand system. Environ. Sci. Technol. 30, 481–488.

Morel, F., Hering, J., 1993. Principles and applications of aquatic chemistry. New York, John Wiley and Sons Inc.

Morshed, J., Kaluarachchi, J.J., 1995. Critical assessment of the operator-splitting technique in solving the advection–dispersion-reaction equation: 2. Monod kinetics and coupled transport. Adv. Water Resour. 18, 101–110.

Öztürk, H.S., Özkan, İ., 2004. Effects of evaporation and different flow regimes on solute distribution in soil. Transp. Porous Media 56, 245–255.

Parkhurst, D.L., Appelo, C.A.J, 1999. User's guide to PHREEQC (Version 2) — A computer program for speciation, batch-reaction, one-dimensional transport and inverse geochemical calculations. Water-Resources Investigations, Report 99-4259, Denver, Co, USA, 312 pp.

Parkhurst, D.L., Kipp, K.L., Engesgaard, P., Charlton, S.C., 2004. PHAST — A program for simulating ground-water flow, solute transport and multicomponent geochemical reactions. U.S.G.S. Techniques and Methods, vol. 6-A8. 154 pp.

Perrochet, P., Berod, D., 1993. Stability and the standard Crank–Nicolson–Galerkin scheme applied to the diffusion–convection equation: some new insights. Water Resour. Res. 29, 3291–3297.

Prommer, H., Barry, D.A., Zheng, C., 2003. MODFLOW/MT3DMS based reactive multi-component transport modelling. Ground Water 41, 247–257.

Saaltink, M.W., Battle, F., Ayora, C., Carrera, J., Olivella, S., 2004. RETRASO, a code for modeling reactive transport in saturated and unsaturated porous media. Geol. Acta 2, 235–251.

Samper, J., Juncosa, R., Delgado, J., Montenegro, L., 2000. CORE^{2D}: A code for nonisothermal water flow and reactive solute transport. User manual version 2. ENRESA Technical Publication 06/2000, 131 pp.

Schäfer, D., Schäfer, W., Kinzelbach, W., 1998. Simulation of reactive processes related to biodegradation in aquifers. 1. Structure of the three-dimensional reactive transport model. J. Contam. Hydrol. 31, 167 186.

Šimůnek, J., Valocchi, A.J., 2002. Geochemical transport, In: Dane, J.H., Topp, G.C. (Eds.), Methods of Soil Analysis, Part 1: Physical Methods, Chapter 6.9, Third ed. SSSA, Madison, WI, pp. 1511–1536.

Šimůnek, J., Šejna, M., van Genuchten, M.Th., 1998. The HYDRUS-1D software package for simulating the one-dimensional movement of water, heat, and multiple solutes in variably-saturated media. Version 2.0, IGWMC-TPS-70, International Ground Water Modeling Center. Colorado School of Mines, Golden, CO. 202 pp.

Stadler, W., 1988. Fundamentals of multicriteria optimization. In: Stadler, W. (Ed.), Multicriteria optimization in Engineering and the Sciences. Plenum Press, New York, pp. 1–25.

Steefel, C.I., 2000. New directions in hydrogeochemical transport modeling: incorporating multiple kinetic and equilibrium pathways. In: Bentley, L.R., Sykes, J.F., Brebbia, C.A., Gray, W.G., Pinder, G.F. (Eds.), Computational Methods in Water Resources XIII. A.A. Balkema, Rotterdam, pp. 331–338.

Steefel, C.I., MacQuarrie, K.T.B., 1996. Approaches to modeling of reactive transport in porous media. In: Lichtner, P.C., Steefel, C.I., Oelkers, E.H. (Eds.), Reactive transport in porous media. Reviews in Mineralogy, vol. 34. Mineralogical Society of America, Washington, DC, pp. 83–129.

Steefel, C.I., Yabusaki, S.B., 1996. OS3D/GIMRT, Software for multicomponent–multidimensional reactive transport, user manual and programmer's guide. PNL-11166, Pacific North West Laboratory, Richland, Washington.

Van Dam, J.C., Feddes, R.A., 2000. Numerical simulation of infiltration, evaporation and shallow groundwater levels with the Richards' equation. J. Hydrol. 233, 72–85.

van der Lee, J., De Windt, L., 2001. Present state and future directions of modeling of geochemistry in hydrogeological systems. J. Contam. Hydrol. 47, 265–282.

van der Lee, J., De Windt, L., Lagneau, V., Goblet, P., 2003. Module-oriented modeling of reactive transport with HYTEC. Comput. Geosci. 29, 265–275.

Vanclooster, M., Viaene, P., Diels, J., Christiaens, K., 1994. WAVE: a mathematical model for simulating water and agrochemicals in the soil and vadose environment, reference and user's manual (release 2.0). Inst. For Land and Water Manage. Katholieke Univ. Leuven, Leuven, Belgium.

van Genuchten, M.Th., 1980. A closed-form equation for predicting the hydraulic conductivity of unsaturated soils. Soil Sci. Soc. Am. J. 44, 892–898.

Walter, A.L., Frind, E.O., Blowes, D.W., Ptacek, C.J., Molson, J.W., 1994. Modeling of multicomponent reactive transport in groundwater. 1. Model development and evaluation. Water Resour. Res. 30, 3137–3148.

Yeh, G.-T., Cheng, H.-P., 1999. 3DHYDROGEOCHEM: A 3-dimensional model of density-dependent subsurface flow and thermal multispecies–multicomponent HYDROGEOCHEMical transport. EPA/600/R-98/159, 150 pp.